THE UNIVERSITY *of* EDINBURGH

Edinburgh Research Explorer

Spontaneously opening GABA receptors play a significant role in neuronal signal filtering and integration

OPEN ACCESS

Cell Death & Disease

ARTICLE

Open Access

Spontaneously opening GABA$_A$ receptors play a significant role in neuronal signal filtering and integration

Nathanael O'Neill[1] and Sergiy Sylantyev [1,2]

Abstract

Continuous (tonic) charge transfer through ionotropic receptors of γ-aminobutyric acid (GABA$_A$Rs) is an important mechanism of inhibitory signalling in the brain. The conventional view has been that tonic GABA-ergic inhibitory currents are mediated by low concentrations of ambient GABA. Recently, however, it was shown that the GABA-independent, spontaneously opening GABA$_A$Rs (s-GABA$_A$Rs), may contribute significantly to the tonic GABA$_A$R current. One of the common approaches to temporal lobe epilepsy (TLE) therapy is an increase of GABA concentration in the cerebrospinal fluid to augment tonic current through GABA$_A$Rs. Such an increase, however, generates multiple side effects, which impose significant limitations on the use of correspondent drugs. In contrast, activation/deactivation of s-GABA$_A$Rs in a GABA-independent manner may provide a mechanism of regulation of tonic conductance without modification of extracellular GABA concentration, thus avoiding connected side effects. Although s-GABA$_A$Rs have been detected in our earlier work, it is unclear whether they modulate neural signalling, or, due to their independence from the neurotransmitter, they provide just a stable background effect without much impact on neural crosstalk dynamics. Here, we focused on the causal relationship between s-GABA$_A$R activity and signal integration in the rat's dentate gyrus granule cells to find that s-GABA$_A$Rs play an important role in neural signal transduction. s-GABA$_A$Rs shape the dynamics of phasic inhibitory responses, regulate the action potential generation machinery and control the coincidence detection window pertinent to excitatory input summation. Our results demonstrate that tonic inhibition delivered by s-GABA$_A$Rs contributes to the key mechanisms that ensure implementation of neural signal filtering and integration, in a GABA-independent manner. This makes s-GABA$_A$R a new and important actor in the regulation of long-term neural plasticity and a perspective target for TLE therapy.

Introduction

The classical trigger of current flow through ionotropic γ-aminobutyric acid receptors (GABA$_A$Rs) is the binding of GABA released from the presynaptic terminal, which induces short, concerted openings of GABA$_A$Rs to mediate phasic inhibition. Another mechanism of inhibitory signalling is charge transfer via tonically (continuously) active GABA$_A$Rs. Studies on tonic inhibitory conductance through GABA$_A$Rs attract substantial attention due to their profound influence on neural excitability, synaptic plasticity, neurogenesis, and network oscillations[1–4]. The relatively understudied form of tonic inhibition is mediated by constitutively active GABA$_A$Rs, i.e., receptors that open spontaneously in the absence of GABA[2].

In our recent study on dentate gyrus granule cells (DGCs), we demonstrated that when the extracellular concentration of GABA was matched to the ambient levels measured in vivo, the vast majority (~90%) of tonic inhibition was delivered by spontaneously opening GABA$_A$Rs (s-GABA$_A$Rs)[5]. s-GABA$_A$Rs do not require the

Correspondence: Sergiy Sylantyev (s.sylantyev@ed.ac.uk)
[1]CCBS, University of Edinburgh, 49 Little France Crescent, Edinburgh EH16 4SB, UK
[2]DCEE, Institute of Neurology, University College London, QSH, Queen Square, London WC1N 3BG, UK
Edited by A. Verkhratsky

SPRINGER **NATURE**
CDD*press*

binding of GABA to enter an active state and, therefore, are resistant to block by competitive antagonists with negligible negative efficacy (SR-95531, SR). However, s-$GABA_AR$s can be inhibited by bicuculline (BIC), which exhibits negative efficacy (inverse agonist)[6] and open-channel blockers, e.g., picrotoxin (PTX) and pentylenetetrazole (PTZ). In the aforementioned study, we showed that SR can reverse the effects of BIC. This important finding demonstrates that the lack of effect of SR-95531 is not simply due to a failure to bind to $GABA_AR$s, but due to the lack of negative efficacy[6].

The hippocampus is a brain area especially prone to epilepsy, and DGCs are commonly affected in a course of temporal lobe epilepsy (TLE) development[7,8]. It was shown that phasic GABA-ergic inhibition is reduced in TLE, whereas the tonic GABA-ergic conductance remains intact[9,10]. This makes tonic GABA-ergic current an attractive target for anti-TLE treatment. The obvious treatment approach is to increase the concentration of extracellular GABA, which activates tonically active $GABA_AR$s. However, this approach was repeatedly found to be ineffective[11,12] or even leading to epileptogenesis[9,13] due to various side effects. In contrast, modulation of s-$GABA_AR$s may offer an alternative approach for the treatment of TLE, by way of augmenting tonic inhibition without the need to change extracellular GABA concentration, thus avoiding the associated off-target effects.

To date, almost nothing is known about the functional impact of this GABA-independent conductance on neuron-firing characteristics and integration of synaptic inputs. In addition, failure to register s-$GABA_AR$s openings in outside-out patches[5] raises a question whether s-$GABA_AR$s activation depends critically from some cytoplasmic factors.

In the present study, we aimed to establish what generic role(s) s-$GABA_AR$s play in regulating the synaptic circuits in the dentate gyrus and provide a new perspective target for TLE therapy. We hypothesized that s-$GABA_AR$s provide a persistent reduction in input resistance, which acts as a break on excitability and narrows the temporal window with which excitatory inputs can be summated to produce an action potential. The dentate gyrus acts as a regulatory "gate" into the hippocampus, serving to filter and separate inputs[14]. Henceforth, even subtle changes to excitability could have a marked effect on the long-term hippocampal plasticity[15]. Lastly, we also tried to clarify if s-$GABA_AR$s are capable of being gated by GABA, as the case in recombinant expression systems[16–18].

Results

s-$GABA_AR$s deliver a major part of inhibitory conductance

As the first step of our study, we assessed whether s-$GABA_AR$s make a significant contribution to the overall inhibitory conductance in DGCs. To distinguish between GABA-dependent and GABA-independent effects of $GABA_AR$s, we used differences in the mechanism of action of SR and PTX. SR has been shown to be a competitive antagonist with no negative efficacy[6] and thus abolishes $GABA_AR$ activity induced by GABA binding, i.e., acts on conventional (GABA-dependent) $GABA_AR$s; conversely, PTX binds inside the $GABA_AR$ channel and thus blocks all $GABA_AR$s that enter active state, i.e., acts on both conventional $GABA_AR$s and s-$GABA_AR$s. Therefore, here and in further experiments, we exploited SR and PTX to measure the activity of conventional $GABA_AR$s and s-$GABA_AR$s. Specifically, conventional $GABA_AR$ activity was assessed as the change in the given effect obtained under control vs. after application of SR, whereas s-$GABA_AR$ activity was measured as the change in the effect obtained after SR application vs. after subsequent application of SR + PTX.

To quantify s-$GABA_AR$ contribution to inhibitory signalling, we performed continuous whole-cell recordings, registering changes in RMS noise (ΔRMS), holding current (ΔI_{hold}) and inhibitory charge transfer (Fig. 1).

SR induced ΔRMS of -0.06 ± 0.04 pA when compared with control value of 3.01 ± 0.26 pA, whereas SR + PTX induced much larger RMS decrease when compared with SR alone: ΔRMS $= -0.49 \pm 0.09$ pA (Fig. 1b). One-way ANOVA demonstrated significant influence of $GABA_AR$ ligands on RMS: $F_{(2,16)} = 4.23$, $P = 0.033$; Student–Newman–Keuls post hoc test (SNK): $P < 0.05$ for Control vs. SR + PTX and for SR vs. SR + PTX.

Similarly, SR induced only a nominal change of -74.9 ± 19.4 pA holding current observed in the control: ΔI_{hold} SR vs. control $= -4.2 \pm 7.3$ pA; on the contrary, the addition of PTX induced much larger effect: ΔI_{hold} SR + PTX vs. SR $= 13.05 \pm 0.97$ pA, Fig. 1b. One-way ANOVA again confirmed significance of $GABA_AR$ ligands effect: $F_{(2,16)} = 4.74$, $P = 0.024$; SNK: $P < 0.05$ for Control vs. SR + PTX and for SR vs. SR + PTX.

When we compared charge transfer through GABA-activated $GABA_AR$s (spontaneous post-synaptic currents, sIPSCs) suppressed by SR and charge transfer through s-$GABA_AR$s suppressed by SR + PTX, we found that s-$GABA_AR$s make a significant contribution to overall inhibitory charge transfer, far surpassing that delivered by sIPSCs: $95.3 \pm 1.2\%$ vs. $4.7 \pm 1.2\%$, $P < 0.0001$, $n = 6$, Student's paired t test (Fig. 1b).

Single-channel properties of s-$GABA_AR$s differ from that of GABA-activated $GABA_AR$s

We next assessed whether s-$GABA_AR$s effects and GABA-triggered effects of $GABA_AR$s can be separated by their single-channel characteristics (conductance, opening frequency and average open-time).

$GABA_AR$ openings were recorded first from the outside-out patch (OOP) and then from the nucleated

Fig. 1 s-GABA$_A$Rs control a major part of inhibitory charge transfer. a Example traces of whole-cell continuous recordings from DGCs. Top: Full experimental trace; application of SR (25 μM) blocks GABA-dependent phasic conductance, whereas subsequent application of SR + PTX (50 μM) blocks tonic conductance controlled by s-GABA$_A$Rs. Horizontal dashed lines mark time intervals over which I_{tonic} was averaged for SR and SR + PTX. Medium: Expanded section of the recording demonstrates the effect of s-GABA$_A$Rs blocked by PTX. Shaded area shows the amount of tonic current controlled by s-GABA$_A$Rs. Bottom: Expanded 0.5-s recording interval before application of SR. Shaded area shows the amount of inhibitory current transferred with GABA-induced phasic events. **b** Statistical summary on effects of s-GABA$_A$Rs and GABA-dependent effects. Top: SR and SR + PTX decrease RMS noise; bars represent change (ΔRMS) from RMS in control (for SR) and from RMS under SR (for SR + PTX), asterisks indicate significance of difference from zero; $n = 6$, Student's paired t test. Medium: Shifts of I_{hold} induced by the application of SR and SR + PTX; ΔI_{hold} for SR and SR + PTX was calculated similarly to ΔRMS. Asterisks indicate significance of difference from zero; $n = 6$, Student's paired t test. Bottom: Input into inhibitory charge transfer delivered by GABA-dependent GABA$_A$Rs (phasic events suppressed by SR) and s-GABA$_A$Rs (tonic response suppressed by SR + PTX). $n = 6$, Student's paired t test. Colour codes apply for all three bar charts, $**P < 0.01$, $***P < 0.001$

patch (NP), pulled from the same neuron (Fig. 2). Application of 10 μM GABA generated single-channel activity in both patch types (Fig. 2a, b). Conversely, in the absence of exogenous GABA, the majority of cells (five out of six) did not exhibit any spontaneous openings in the OOP configuration. However, with low-impedance pipettes (~3 MΩ), we could detect GABA-independent openings in OOPs.

Fig. 2 s-GABA$_A$Rs can be distinguished from conventional GABA$_A$Rs by opening frequency and average open-time. a Example trace of single-channel activity in the membrane patch with a sequence of GABAR ligand application. **b** Single-channel GABA$_A$Rs openings in membrane patches. Left: outside-out patch. Right: nucleated patch, pulled from the same neuron. "C" and "O" denote closed and open states of the receptor, respectively. Arrow indicates low-conductance receptor opening. Traces from top to bottom: GABA (10 μM), perfusion solution without GABA$_A$R ligands, GABA (10 μM) + SR (25 μM) and GABA (10 μM) + PTX (50 μM). Scale bars apply to all traces. **c** Statistical summary on single-channel parameters recorded in **b**. Asterisks show significance of difference from the value generated by GABA only at corresponding patch type. *$P < 0.05$, **$P < 0.01$, ***$P < 0.001$, $n = 6$, Student's paired *t* test. **d** All-points open-time histograms for receptor openings recorded in **b**. Axes legends apply to all histograms. OOP: outside-out patch, NP: nucleated patch

In both OOPs and NPs, the absence of GABA and the application of SR (25 μM) left intact the part of the single-channel activity, whereas PTX (50 μM) blocked it in full (Fig. 2b).

Single-channel conductance was indistinguishable in OOPs and NPs under all experimental conditions (varying from 38.3 ± 1.3 to 36.9 ± 1.9 pS, Fig. 2c), which does not allow distinguishing s-GABA$_A$Rs from GABA-activated

GABA$_A$Rs. Instead, s-GABA$_A$Rs can be isolated pharmacologically by withdrawal of GABA and/or application of SR, which cause a significant decrease in the receptor-opening frequency and average open-time. In OOPs, the opening frequency decreased from 15.6 ± 3.1 Hz obtained with GABA in the perfusion solution to 2.98 ± 1.78 Hz without GABA ($P = 0.0084$, $n = 6$, Student's paired t test), and to 2.02 ± 1.23 Hz under SR ($P = 0.0092$, $n = 6$, Student's paired t test). In NPs, the opening frequency decreased from 19.98 ± 1.84 Hz generated by GABA to 5.54 ± 1.92 Hz and 4.42 ± 2.64 Hz when GABA was withdrawn and SR was added ($P = 0.0089$ and $P = 0.0071$, respectively, $n = 6$ in both cases, Student's paired t test). The average open-time was also significantly decreased by pharmacological interventions: in OOPs, from 33.93 ± 5.1 ms under GABA to 16.37 ± 2.78 ms with no GABA, and 14.35 ± 2.85 ms under SR ($P = 0.038$ and $P = 0.029$, respectively, $n = 6$, Student's paired t test). In NPs, the average open-time decreased from 27.24 ± 3.76 ms under GABA to 15.92 ± 2.96 ms with no GABA, and 14.27 ± 2.6 ms with SR ($P = 0.041$ and $P = 0.037$, respectively, $n = 6$ for both cases, Student's paired t test; Fig. 2c).

To probe single-channel GABA$_A$R properties deeper, we generated all-points open-time histograms for channel openings (Fig. 2d). Histograms for recordings in the presence of GABA were best fitted with the double-Gaussian function; mode values 11.8 ± 2.22 and 33.9 ± 5.1 ms for OOPs, 13.9 ± 4.4 and 36.9 ± 7.8 ms for NPs. In the latter case, the plot clearly displayed two distinct peaks. In contrast, under all other experimental conditions, the histograms were best fitted with a single-Gaussian function. Mode values for OOPs without GABA (15.26 ± 2.71 ms), NPs without GABA (14.86 ± 2.84 ms), OOPs with SR (15.48 ± 2.92 ms) and NPs with SR (13.58 ± 2.42 ms) displayed no significant difference from the lower-mode value obtained with GABA for OOPs and NPs, respectively ($P > 0.3$, $n = 6$ and 6; Student's t test for all comparisons). Our further tests proved that changes in single-channel response characteristics were not due to the side effects of GABA$_A$R ligands[19,20] (Fig. 3 and Supplementary Section 1).

s-GABA$_A$Rs modulate IPSC kinetics

Next, we asked whether s-GABA$_A$Rs can be activated by the synaptic GABA efflux. To assess this, we tested whether and to what extent does s-GABA$_A$Rs shape IPSC kinetics. Our working hypothesis was that s-GABA$_A$Rs are sensitive to GABA, and IPSC decay profiles should consist of two exponents, with one exponent generated predominantly by s-GABA$_A$Rs and another predominantly by conventional GABA$_A$Rs. To distinguish between the effects produced by the two receptor subtypes, we again used difference in action mechanisms of SR and PTX. We presumed that in the solution

containing PTX, but not GABA, PTX would gradually block s-GABA$_A$Rs, binding inside the ion channels when they open spontaneously, but leave intact the conventional GABA$_A$Rs, since they open only after GABA binding. If after incubation in PTX, a pulse of GABA arrives, the ratio of fitting coefficients (RFC) of two IPSC decay exponents should be biased in favour of GABA-dependent GABA$_A$Rs (see Fig. 4d legend for more details). In turn, the incubation in SR with subsequent GABA + SR pulse should suppress equally the effect of conventional GABA$_A$Rs and s-GABA$_A$Rs.

To test the hypothesis, we performed a rapid solution application experiment (Fig. 4). Since it is virtually impossible to wash out PTX from GABA$_A$Rs during the characteristic lifetime of NP (3–7 min), the sequence of ligands application was first set as: GABA (2 mM)— GABA (2 mM) + SR (0.2 mM)—2–3 min incubation in PTX (50 µM)—GABA (2 mM).

Bi-exponential fitting of response-decay profiles generated in NPs by GABA after incubation in PTX displayed a higher RFC, compared with responses generated under control: 3.83 ± 0.78 vs. 1.79 ± 0.34, $P = 0.037$, $n = 9$, Student's paired t test. However, the RFC of responses generated by GABA + SR unexpectedly displayed significantly lower values than that generated by the pure GABA: 1.14 ± 0.23 vs. 1.79 ± 0.34, $P = 0.042$, $n = 9$, Student's paired t test (Fig. 4c–f).

Thus, we found that PTX and SR change the RFC of GABA-generated phasic response in opposite directions. But, were both effects generated by s-GABA$_A$Rs? To clarify this, we again used the phenomenon of high-affinity binding of PTX to GABA$_A$R. In the absence of GABA, PTX should selectively and almost irreversibly block s-GABA$_A$Rs; thus, if the effect of SR does not develop after removal of PTX from the perfusion solution, this would mean that the SR-generated bias under control was due to s-GABA$_A$Rs.

Therefore, we repeated the experiment with a modified sequence of the applied solutions: GABA, incubation in PTX (3 min), GABA + SR. Indeed, this prevented the development of SR-generated deceleration of decay kinetics; the RFC generated by GABA + SR did not differ significantly from that generated by pure GABA: 2.72 ± 0.49 vs. 1.86 ± 0.52, $P = 0.22$, $n = 6$, Student's paired t test (Fig. 4c–f).

In contrast to NPs, pharmacological manipulations had no significant effect on RFC obtained for OOPs (Fig. 4e–g): $P > 0.4$ for all comparisons, $n = 6–9$, Student's paired t test. This suggests the critical role of cytoplasmic factors in the development of GABA-dependent effects of s-GABA$_A$Rs on IPSC kinetics.

GABA$_A$R antagonists did not cause a significant effect on the absolute values of IPSC decay time constants and, predictably, lowered the response amplitudes (Supplementary Section 2).
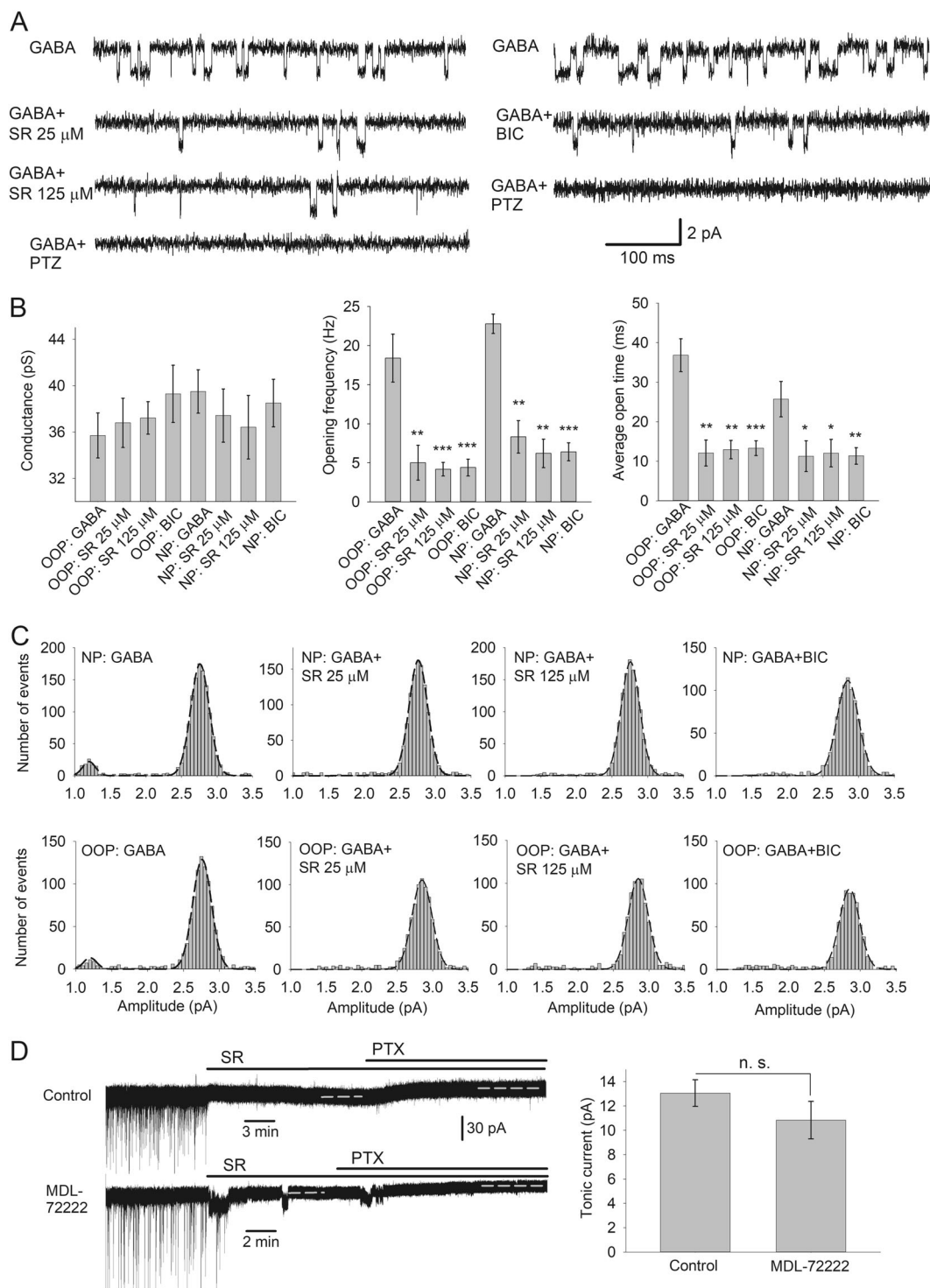
Fig. 3 No significant side effects are generated by GABA$_A$R ligands. a Example traces of single-channel GABA$_A$Rs openings in membrane patches. Left: Effects of incrementing concentrations of SR and PTZ (100 µM). Right: Effects of BIC (50 µM) and PTZ (100 µM). Scale bars apply to all traces. **b** Statistical summary on single-channel parameters recorded in **a**. Asterisks show significance of difference from the value generated by GABA only at the corresponding patch type. *$P < 0.05$, **$P < 0.01$, ***$P < 0.001$, $n = 6$, Student's paired t test. **c** Response amplitude histograms for receptor openings recorded in **a**. Axes legends apply to all histograms. OOP: outside-out patch, NP: nucleated patch. Note, generation of lower-conductance openings only in patches exposed to pure GABA; to improve histogram quality, recordings with GABA$_A$Rs antagonists continued 3–6 times longer than that with pure GABA. **d** 5HT$_3$ receptor antagonist MDL-72222 (10 µM) has no significant effect on charge transfer through s-GABA$_A$Rs. Left: Example traces of whole-cell recordings. Vertical scale bar applies to both traces. Horizontal dashed lines mark the time intervals over which I_{tonic} was averaged for SR and SR + PTZ. Right: Statistical summary. $n = 6$ and 6; Student's unpaired t test
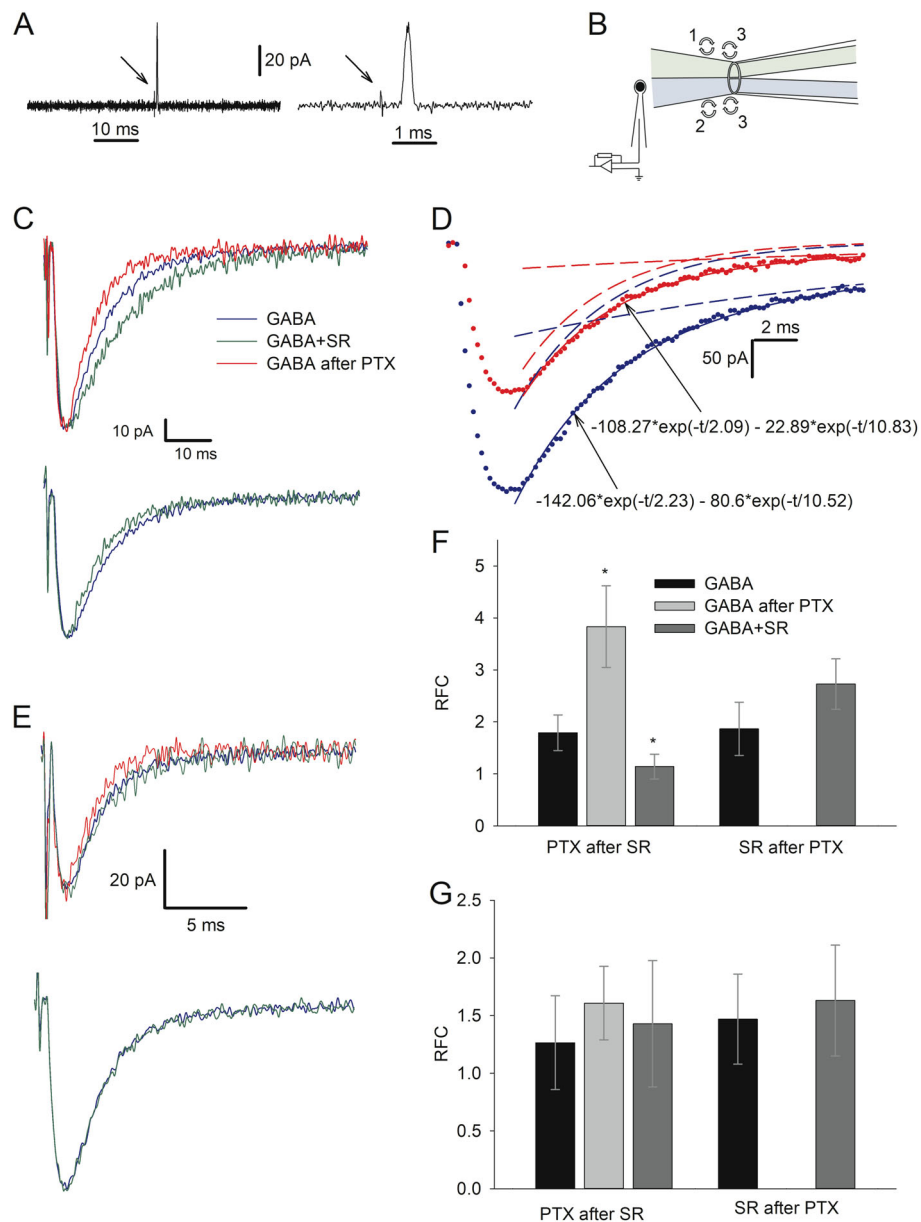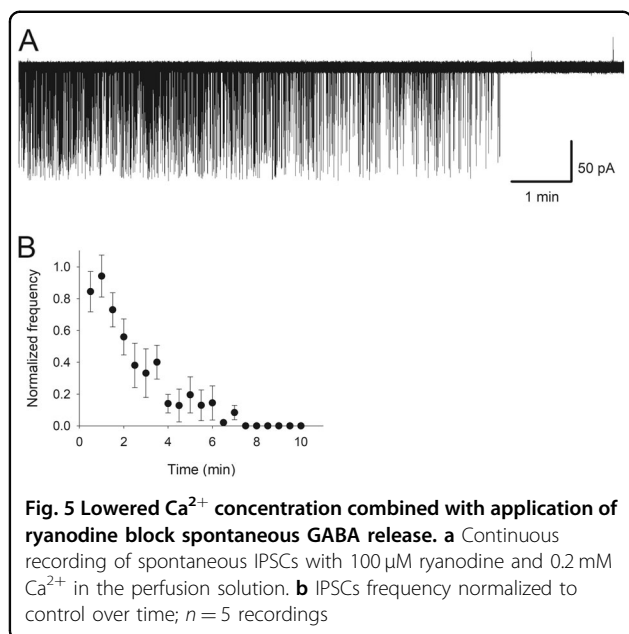
Fig. 4 s-GABA_ARs modulate IPSC kinetics in nucleated patches, but not in outside-out patches. a Open-pipette test of solution exchange time at long (left) and short (right) time scale. Distilled water (with lower conductivity) and aCSF swap at the recording pipette tip with a time constant of 50–100 µs. Arrows point to electrical switch artefact; vertical scale bar applies to both traces. **b** Illustration of rapid solution application system (schematic) with θ-glass pipette, which applies two different solutions at NP placed at a patch pipette. Numbers denote sequence of drug cocktail replacements in θ-glass pipette channels: 1—GABA → GABA + SR; 2—aCSF with no GABA_AR ligands → aCSF with PTX; 3—GABA + SR → GABA and aCSF with PTX → aCSF with no GABA_AR ligands. During solution replacement time periods, the patch was exposed to the solution flowing from the "bottom" channel. **c** Inhibitory currents generated in NPs in response to short-term application of GABA_ARs ligands. Sequence of solution switches for top panel (three traces): no ligands—GABA (2 mM); SR (200 µM)—GABA + SR; incubation in PTX (25 µM); no ligands—GABA. For bottom panel (two traces): no ligands—GABA; incubation in PTX; SR—GABA + SR. Responses were normalized to peak amplitude of response generated by GABA in "no ligands—GABA" switch; each response is an average of 3–6. GABA_AR ligands in applied solution are colour-coded, codes apply to **c**–**e**. **d** Analysis paradigm for response-decay kinetics with double-exponential fitting. Solid lines through data points: best-fit double-exponential functions; dashed lines of the same colour are plots of the fast and slow components alone. Blue: application of GABA; red: application of GABA after incubation in PTX. Decay components ratio of fast ($\tau = 2.23$) to slow ($\tau = 10.52$) component generated by GABA was obtained as 142.06/80.6 = 1.76; incubation in PTX-augmented decay components ratio to 108.27/22.89 = 4.73. **e** Same as **c**, but solutions applied at OOP. **f** Statistical summary on ratios of fitting coefficients (RFC) for recordings from NPs. Colour codes apply to **f** and **g**. **g** Statistical summary on RFC for recordings from OOPs. Asterisks denote significance of difference from ratio generated by GABA in "no ligands—GABA" switch; *$P < 0.05$, $n = 6$, Student's paired *t* test

Fig. 5 Lowered Ca²⁺ concentration combined with application of ryanodine block spontaneous GABA release. a Continuous recording of spontaneous IPSCs with 100 μM ryanodine and 0.2 mM Ca^{2+} in the perfusion solution. **b** IPSCs frequency normalized to control over time; $n = 5$ recordings

To further test the working hypothesis under more physiological conditions, we studied the whole-cell response kinetics in acute hippocampal tissue, where the GABA-ergic responses were induced by electrical stimulation of the perforant path. Here we combined the application of ryanodine and lowered Ca^{2+} concentration to prevent the block of GABA-dependent GABA$_A$Rs due to spontaneous transmitter release during incubation in PTX (Fig. 5 and Supplementary Section 3).

As expected, the application of 50 μM PTX for 5 min generated significant increase of RFC compared with control: 3.12 ± 0.22 vs. 2.38 ± 0.29, $P = 0.038$, $n = 11$, Student's paired t test. In turn, SR induced significant deceleration of the IPSC kinetics: RFC 1.54 ± 0.34 vs. 2.38 ± 0.29, $P = 0.039$, $n = 10$, Student's paired t test (Fig. 6). Again, pre-incubation in PTX prevented the SR effect, thus demonstrating its generation by s-GABA$_A$Rs: RFC 2.27 ± 0.64 when SR was added after PTX vs. 2.09 ± 0.45 under control, $P = 0.71$, $n = 6$, Student's paired t test (Fig. 6b).

s-GABA$_A$Rs regulate AP generation and signal integration properties of DGCs

Since s-GABA$_A$Rs input in whole cell is sufficient for significant impact on response kinetics (Fig. 6) and neuronal excitability (Fig. 7 and Supplementary Section 4), we next asked whether s-GABARs modulate the action potential (AP) generation. To clarify this, we injected increasing amounts of depolarizing current and recorded the frequency of the generated APs at each current step (Fig. 8a). We found that both SR and SR + PTX significantly biased the "current–frequency" relationship. Two-way ANOVA with GABA$_A$R ligands (SR 25 μM and
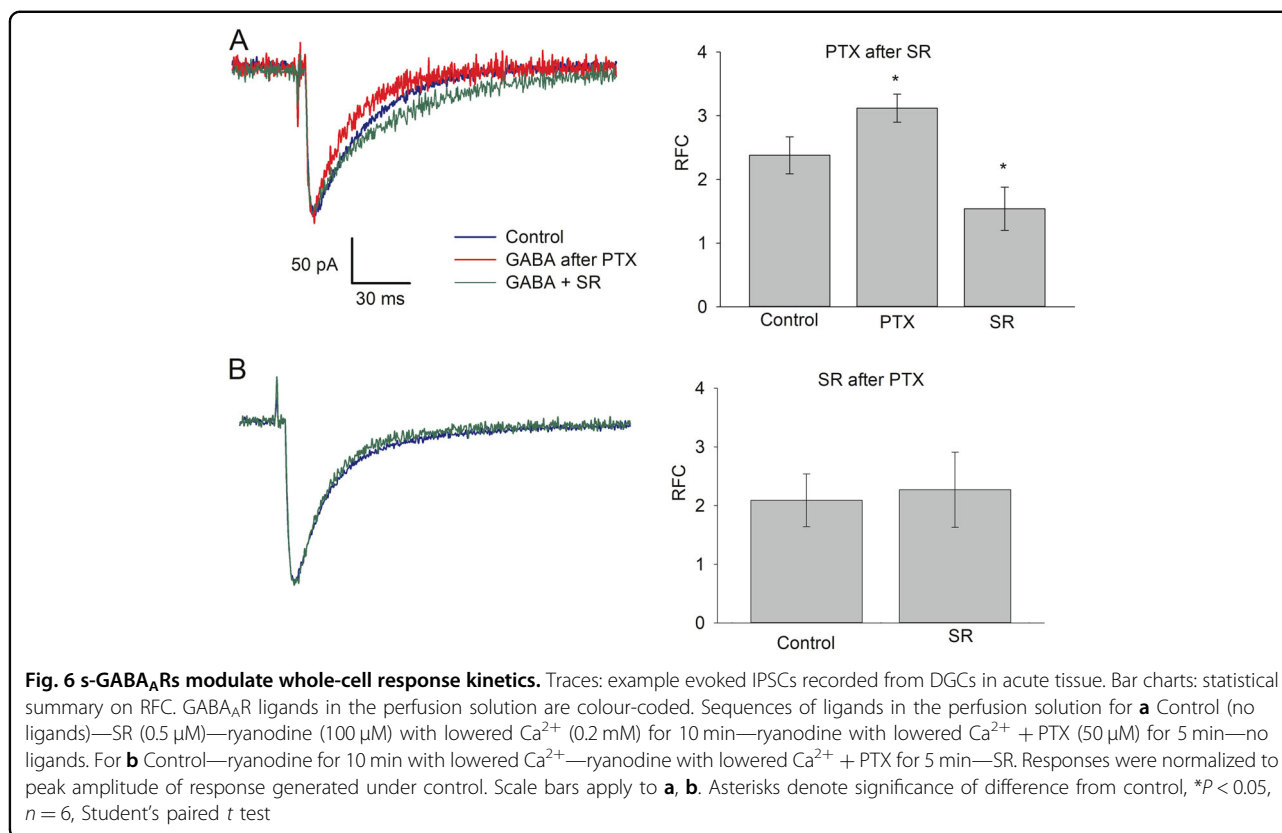
SR 25 μM + PTX 50 μM) effect as factor 1 and injected amperage as factor 2 demonstrated highly significant impact of both factors on cell-firing frequency. For factor 1: $F_{(2,240)} = 46.83$, $P = 6.73 \times 10^{-18}$; SNK: $P < 0.05$ for all paired comparisons. For factor 2: $F_{(10,240)} = 55.36$, $P = 1.06 \times 10^{-56}$; SNK: $P > 0.05$ for data groups at 0, 25 and 50 pA. For factor 1 × factor 2: $F_{(20, 240)} = 2.34$, $P = 0.0014$.

Finally, to illustrate the role of s-GABA$_A$Rs in signal integration, we performed a coincidence detection experiment (Fig. 8b). Here the probability of spiking under control conditions rapidly decreased when one of two stimuli was shifted in time from another with 2.5 ms steps; a Gaussian fit gave the standard deviation value as $\sigma = 4.1 \pm 1.3$ ms ($n = 6$ cells). We then repeated the stimulation protocol (with 5 ms steps) with SR (25 μM) and SR + PTX (50 μM) in perfusion solution. The SR significantly prolonged the integration time window: $\sigma = 8.7 \pm 1.8$ vs. $\sigma = 4.1 \pm 1.3$ in control, $P = 0.036$, $n = 5$ and 6, Student's t test. In turn, SR + PTX significantly prolonged integration window compared to SR alone: $\sigma = 12.6 \pm 1.7$ vs. $\sigma = 8.7 \pm 1.8$, $P = 0.044$, $n = 6$ and 5, Student's t test.

Discussion

In the present study, we performed a detailed research of the s-GABAAR-mediated tonic inhibition and revealed that these receptors provide the vast majority of tonic GABA-independent inhibitory conductance in DGCs. The functional consequence of s-GABAR conductance is to alter the basic membrane properties, shape IPSC kinetics, perturb excitability and narrow the temporal window of coincidence detection.

The significant input of s-GABA$_A$Rs in inhibitory conductance of the DGCs (Fig. 1b) makes these receptors an important actor regulating signal filtering, and potentially a perspective drug target. However, was this tonic current delivered purely by s-GABA$_A$Rs, but not by GABA$_A$Rs, that bind GABA with a high-enough affinity to prevent it from being displaced by SR? Two observations suggest that the latter is not the case. First, in our previous study, we demonstrated that 25 μM of SR do not cause significant decrease of tonic conductance in DGCs compared to the effect of 0.5 μM[5]. Taking into account SR's EC$_{50}$ of ~0.15 μM[21], the 25 μM concentration used in this study is very likely saturating all GABA-dependent GABA$_A$Rs. This was further confirmed in our experiment, where the effects of SR 25 and 125 μM did not differ significantly (Fig. 3). Second, we have also shown previously that SR at the concentration 25 μM fully removes BIC effects generated at s-GABA$_A$Rs[5]. Another explanation of the s-GABA$_A$R current under SR could be that GABA$_A$Rs of specific subtype exhibit a weak agonist response to SR. Single-channel recordings allowed us to clarify this point: application of SR together with GABA left s-GABA$_A$Rs active, but did not trigger significant changes in s-
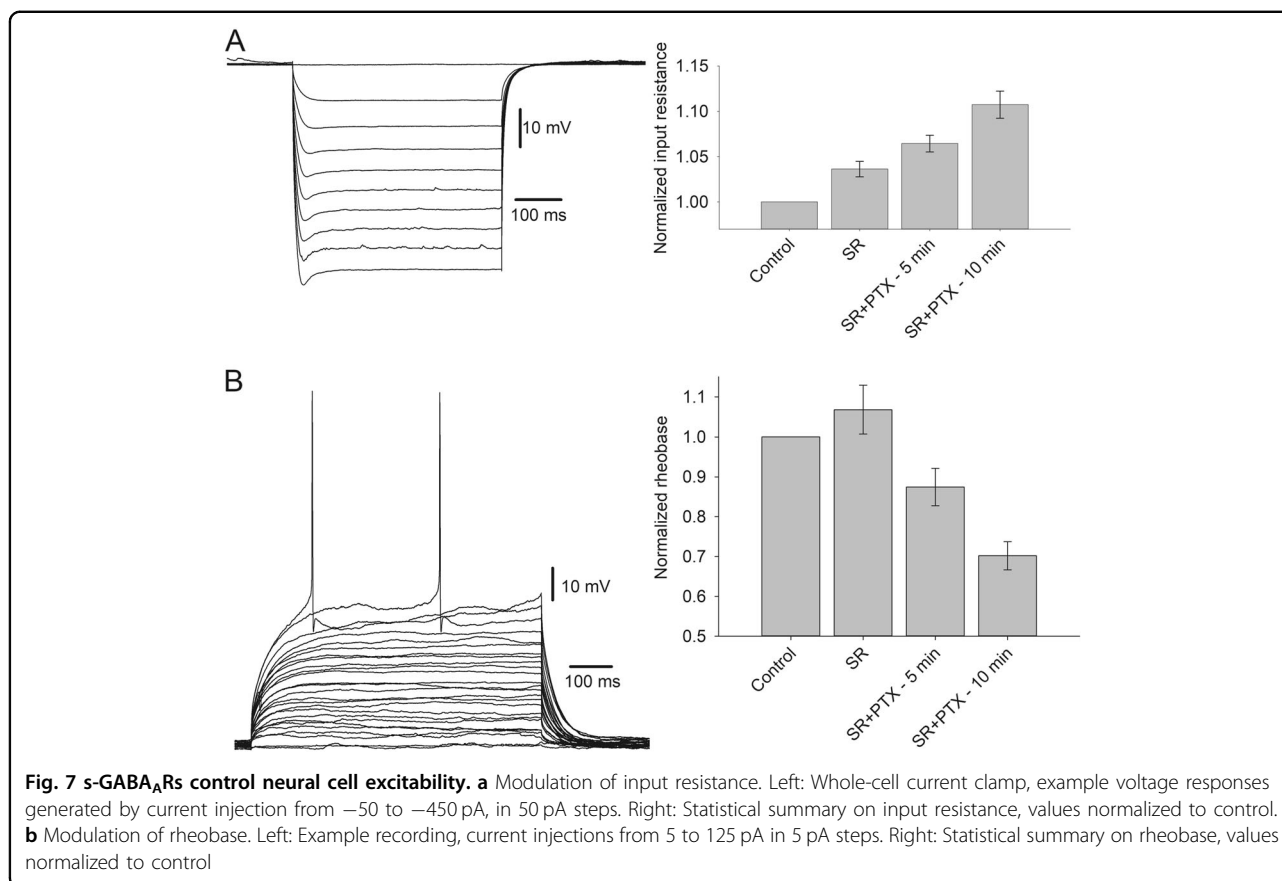
Fig. 6 s-GABA$_A$Rs modulate whole-cell response kinetics. Traces: example evoked IPSCs recorded from DGCs in acute tissue. Bar charts: statistical summary on RFC. GABA$_A$R ligands in the perfusion solution are colour-coded. Sequences of ligands in the perfusion solution for **a** Control (no ligands)—SR (0.5 μM)—ryanodine (100 μM) with lowered Ca^{2+} (0.2 mM) for 10 min—ryanodine with lowered Ca^{2+} + PTX (50 μM) for 5 min—no ligands. For **b** Control—ryanodine for 10 min with lowered Ca^{2+}—ryanodine with lowered Ca^{2+} + PTX for 5 min—SR. Responses were normalized to peak amplitude of response generated under control. Scale bars apply to **a**, **b**. Asterisks denote significance of difference from control, *$P < 0.05$, $n = 6$, Student's paired *t* test

GABA$_A$Rs opening frequency and average open-time compared to those obtained without GABA$_A$R ligands in perfusate (Fig. 2b, c). GABA concentration in this experiment (10 μM) was ~100 times higher than the native found in dentate gyrus[5]. This confirms that that 25 μM of SR are sufficient to displace GABA from GABA$_A$Rs, but do not modify s-GABA$_A$Rs conductance.

In this paper, we extended the previous findings on single receptor openings: s-GABA$_A$Rs can be distinguished from the pool of conventional GABA$_A$Rs as having shorter average open-time and lower opening probability, however, they have similar conductance (Figs. 2 and 3). The double-Gaussian distribution of single-channel open-time intervals generated by GABA in NPs (Fig. 2d) indicates the presence of two functionally distinct populations of receptors. It is worth to note that the double-Gaussian optimal fit of single-channel open-time distributions was demonstrated earlier for at least three different GABA$_A$R subunit compositions[22], with similar mode value for shorter durations, irrespective of the agonist's type and concentration. This represents an agonist-independent input, which resembles our observations and suggests that s-GABA$_A$R activity is a common element of GABA$_A$R-generated inhibitory current originating from GABA$_A$Rs of various subunit compositions.

s-GABA$_A$Rs in OOPs have been reported previously for hippocampal primary neurons[6], but to the best of our knowledge, not for DGCs. The presence of s-GABA$_A$R openings in NPs and their absence in OOPs demonstrated in earlier work[5] suggested critical dependence of the GABA-independent activity in DGCs on cytoplasmic factors. However, here we successfully recorded s-GABA$_A$R's spontaneous openings in OOPs using low-impedance patch pipettes; thus, the inability to register them in earlier studies was probably due to s-GABA$_A$R's low density on cell soma, aggravated by the tendency of GABA$_A$Rs to cluster[23].

When GABA$_A$Rs are activated by GABA pulse, the block of s-GABA$_A$Rs with PTX suppressed the slow component of the decay profile more than the fast one (Fig. 4), and the block of GABA binding with SR suppressed the fast component more than the slow one. This effect of SR, however, did not develop when s-GABA$_A$Rs were deactivated by pre-incubation in PTX (Figs. 4 and 6), thus proving the SR-induced suppression of the fast component to be generated by s-GABA$_A$Rs. On top of a general proof of ability of s-GABA$_A$Rs to be activated by GABA, this observation suggests that, when activated by GABA, s-GABA$_A$Rs have different single-channel response characteristics compared to their spontaneous

Fig. 7 s-GABA$_A$Rs control neural cell excitability. a Modulation of input resistance. Left: Whole-cell current clamp, example voltage responses generated by current injection from −50 to −450 pA, in 50 pA steps. Right: Statistical summary on input resistance, values normalized to control. **b** Modulation of rheobase. Left: Example recording, current injections from 5 to 125 pA in 5 pA steps. Right: Statistical summary on rheobase, values normalized to control

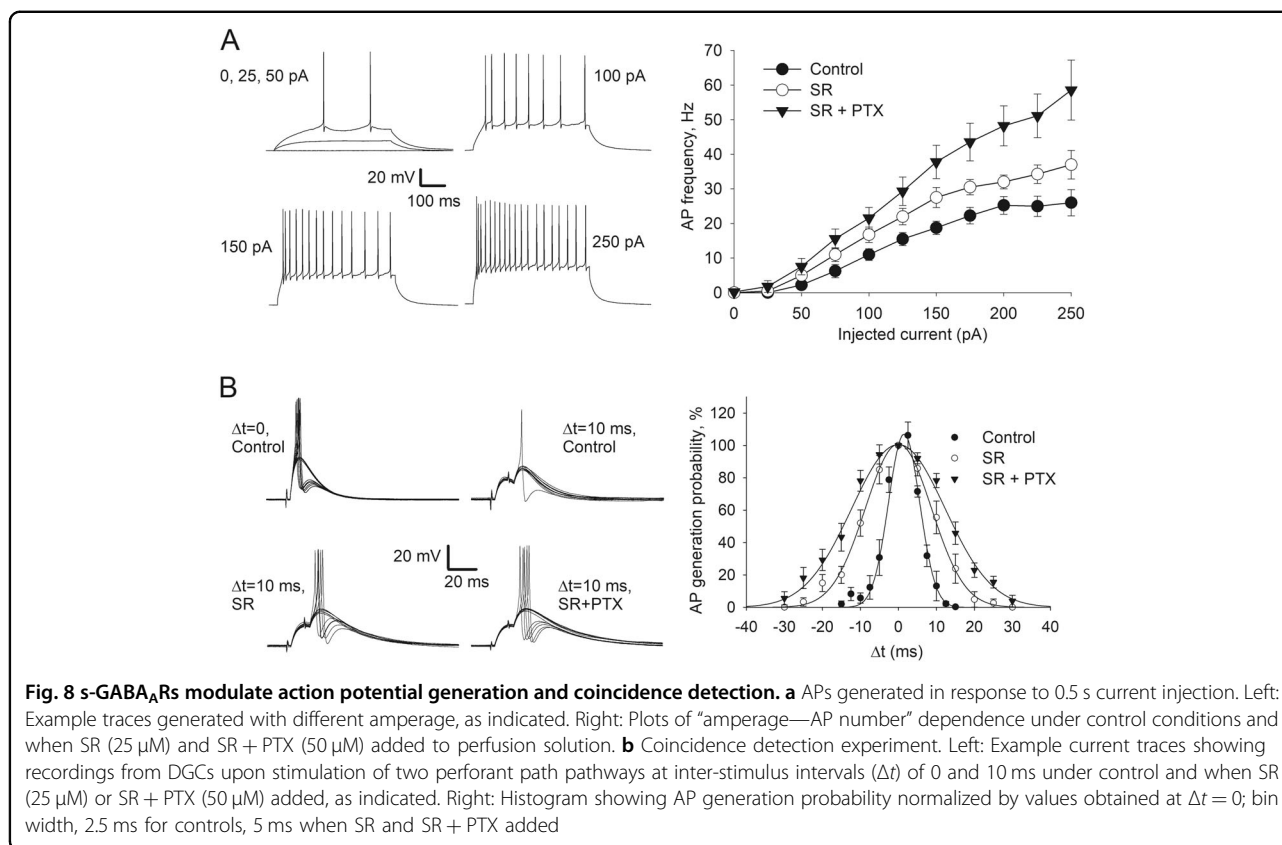activity state, and/or have higher affinity to GABA than the conventional GABA$_A$Rs.

Studies on network signalling in the hippocampus have shown DGCs to be linear integrators of synaptic inputs coming from the entorhinal cortex[24]. To match this role, DGCs should act as strong EPSP attenuators with a high AP threshold[24,25]. Therefore, inhibition delivered by s-GABA$_A$Rs, which narrows an integration window for excitatory inputs (Fig. 8b), is a key mechanism that ensures implementation of the main functional role of DGCs.

Subunit selective GABA$_A$R ligands are widely recognized to be a perspective class of compounds for exploring and validating potential anti-epileptic drugs allowing fine-tuning of TLE therapy[26,27]. Therefore, an important question to be addressed in future studies is, which GABA$_A$R subunit(s) turns conventional GABA$_A$Rs to s-GABA$_A$Rs? It has been demonstrated that scarcity of α1 subunit is correlated with resistance to anti-epileptic drugs[28], whereas increased α1-GABA$_A$R expression in hippocampus suppresses TLE development[8]. α1 subunit when incorporated into GABA$_A$Rs has been shown to modulate spontaneous GABA$_A$Rs gating[29], thus making α1-GABA$_A$R a good candidate for generation of at least a part of s-GABA$_A$Rs effects. Positive allosteric GABA$_A$R

modulator zolpidem selectively increases the activity of α1-subunit-containing GABA$_A$Rs partially in GABA-independent manner[30]. Apart of α1-GABA$_A$R, another possible candidate to be a part of s-GABA$_A$Rs functional group is α5-containing GABA$_A$R: it was shown to generate SR-insensitive component of phasic current[31] and contribute to tonic conductance[32]. Compounds such as zolpidem and propofol, which upregulate s-GABA$_A$Rs activity in GABA-independent manner[6,30], maybe thus be useful candidates to counteract TLE development.

It has long been established that amount of Cl$^-$ current transfer through GABA$_A$Rs has a bell-shaped dependence on temperature in a physiological temperature range[33,34]. This is specifically important for DGCs, where rise of temperature from 22–23 to 34–36 °C generates approximately twofold increase of tonic current[35]. On top of that, increase of temperature augments zolpidem-modulated inhibitory current through α1-GABA$_A$Rs to a higher extent than the inhibitory current through zolpidem-insensitive GABA$_A$Rs[36]. This may suggest that s-GABA$_A$Rs of DGCs (selectively modulated by zolpidem) are one of the main factors implementing temperature-dependent control over inhibitory current.

Abnormal increase of intracellular Cl$^-$ concentration was found earlier to slow down GABA$_A$R IPSC kinetics, in

Fig. 8 s-GABA_ARs modulate action potential generation and coincidence detection. a APs generated in response to 0.5 s current injection. Left: Example traces generated with different amperage, as indicated. Right: Plots of "amperage—AP number" dependence under control conditions and when SR (25 µM) and SR + PTX (50 µM) added to perfusion solution. **b** Coincidence detection experiment. Left: Example current traces showing recordings from DGCs upon stimulation of two perforant path pathways at inter-stimulus intervals (Δt) of 0 and 10 ms under control and when SR (25 µM) or SR + PTX (50 µM) added, as indicated. Right: Histogram showing AP generation probability normalized by values obtained at $\Delta t = 0$; bin width, 2.5 ms for controls, 5 ms when SR and SR + PTX added

particular, in IPSCs generated by α1-containing GABA_ARs, and to modulate neuron-firing probability[37]. This raises a question whether and to what extent s-GABA_ARs effects observed in our work were dependent from Cl^- concentration. Indeed, IPSC deceleration generated by s-GABA_ARs in our voltage-clamp recordings was observed under 128.5 mM intracellular Cl^- (see Methods), which is much higher than physiological concentration and implies existence of Cl^--generated bias. However, in current-clamp experiments, s-GABA_ARs caused a significant impact on neuronal firing under 4 mM intracellular Cl^-, which is close to the lower limit of physiological concentrations typically found in neurons (~5–10 mM[37]). Therefore, s-GABA_ARs effects in our preparation cannot be reduced to impact intracellular Cl^- concentration on inhibitory transmission.

Both α1- and α5-GABA_AR are modulated by a number of cytoplasmic proteins[38–40], which are controlled by G protein-delivered signalling triggered by glutamate and GABA_B receptors[41–43]. Therefore, permanent block of GABA_B and glutamate receptors in our study may exert a stable background effect, which modifies quantitative outcome of s-GABA_ARs activation. This points to cytoplasmic actors as to one of the further research directions that allows comprehension of s-GABA_ARs functioning.

Methods and materials
Hippocampal slice preparation

Transverse hippocampal slices (350–400 µM thick) were used for in vitro electrophysiological recordings. Slices were prepared from 3- to 5-week-old female Sprague Dawley rats. Animals were killed by cervical dislocation after being anesthetized by an overdose of isoflurane, according to the United Kingdom Animals (Scientific Procedures) Act of 1986. After decapitation, brains were rapidly removed and dissected, and whole-brain sagittal slices were prepared with a Leica VT1200S vibratome in semi-frozen sucrose-based solution containing the following (in mM): 70 sucrose, 80 NaCl, 2.5 KCl, 4 MgCl_2, 0.5 CaCl_2, 15 NaHCO_3, 10 HEPES, 1.25 NaH_2PO_4 and 22 glucose, equilibrated with 95% O_2 plus 5% CO_2, pH 7.35, 315–330 mOsm. Slices were placed in continuously oxygenated sucrose-aCSF at 35 °C for 20 min and then allowed to recover for a further 30 min at room temperature before recording. Individual slices were then transferred into recording chamber and perfused with standard ACSF containing (in mM): 119 NaCl, 2.5 KCl, 1 MgCl_2, 2.5 CaCl_2, 10 HEPES, 15 NaHCO_3, 1.25 NaH_2PO_4 and 22 glucose, and was continuously gassed with 95%O_2 and 5%CO_2, pH 7.35; 290–298 mOsm. aCSF temperature during experiments was held at 33 °C, under the control of an inline heater.

Electrophysiology

Whole-cell recordings

Visualized patch-clamp recordings from mature dentate granule cells were performed using an infra-red differential interference contrast imaging system. Tonic GABA$_A$R-mediated currents were measured in voltage-clamp mode at holding potential $V_{hold} = -70$ mV at 33 °C in the presence of ionotropic glutamate receptor blockers, DL-APV (50 μM) and NBQX (20 μM), metabotropic glutamate receptors blocker, (S)-α-methyl-4-carboxyphenylglycine (MCPG; 250 μM) or N-tricyclo-[3.3.1.13,7]-dec-1-yl-2-qui-noxalinecarboxamide (NPS; 10 μM) plus (RS)-α-Cyclopro-pyl-4-phosphonophenylglycine (CPPG; 5 μM), glycine receptor blocker, strychnine (1 μM) and GABA$_B$ receptor blocker (2S)-3-[[(1S)-1-(3,4-dichlorophenyl)ethyl]amino-2-hydroxypropyl](phenylmethyl) phosphinic acid (CGP55845; 1 μM). The intracellular pipette solution for voltage-clamp experiments contained the following (mM): 120.5 CsCl, 10 KOH-HEPES, 2 EGTA, 8 NaCl, 5 QX-314 Br$^-$ salt, 2 Mg-ATP and 0.3 Na-GTP; for current-clamp experiments, it contained 126 K-gluconate, 4 NaCl, 5 HEPES, 15 glucose, 1 MgSO$_4$·7H$_2$O, 2 BAPTA and 3 Mg-ATP; pH adjusted to 7.2 and osmolarity adjusted to 295 mOsm. Competitive antagonist SR-95531 (SR) and channel blocker picrotoxin (PTX) were used to apply partial and full block of GABA$_A$Rs activity, respectively. Recordings were performed at 32–34 °C; the patch pipette resistance was 2–4 MΩ for whole-cell recordings and 3–7 MΩ for recordings from outside-out and nucleated patches. Series resistance was monitored throughout the experiments using a +5 mV step command; cells with unstable series resistance (above 25 MΩ) or unstable holding current were rejected. To stimulate the hippocampal neural tissue, electrical stimuli were delivered through bipolar-stimulating electrode placed in perforant path. Constant voltage DS2A stimulus isolators (Digitimer LTD) were used to deliver electrical stimuli to neural tissue during whole-cell recordings and activate piezoelectric actuator in rapid solution application experiments on membrane patches.

Outside-out and nucleated patch recordings

Outside-out patches (OOPs) and cell membrane bags containing intact nucleus and cytoplasm (nucleated patches, NPs) were pulled from dentate gyrus granule cells, and recordings were performed in voltage-clamp mode (V_{hold} −70 mV). Rapid solution exchange experiments were performed as described in our earlier published protocol[44]. Briefly, we used a θ-glass application pipette, with ~200 μm tip diameter attached to the micro-manipulator. The position of the pipette was controlled by piezoelectric element, the switch time constant was 50–100 μs. One pipette channel was filled with the bath aCSF solution and another channel had GABA or GABA plus antagonist (SR or PTX). Pressure was regulated by a PDES-02DX pneumatic micro ejector (npi), using compressed nitrogen separately in each of the two channels. Solutions with GABA, GABA + SR and GABA + PTX were exchanged in a pipette channel in 7–12 s[44]; after replacement of solutions, the following series of rapid applications of one type of solution takes about 15–30 s. Therefore, since GABA$_A$Rs response recovery after PTX application requires a washout for the time period from 10–15 min[45] to several tens of minutes[46,47], we presumed that at least a large part of s-GABA$_A$Rs remains blocked by PTX during the <1 min full experimental cycle.

To prevent contamination with the spilled over GABA released from neural tissue, continuously recorded membrane patches were placed in a solution current flowing from the motionless θ-glass pipette, where stable concentrations of GABA$_A$R ligands were maintained.

There are several technical problems that affect data interpretation in this type of experiments. First, due to the large difference in surface area between the membrane patches (especially between NPs), the number of individual ion channels, in particular, patches may vary up to an order of magnitude, with corresponding effect on the response amplitude. Another technical complication of the rapid solution exchange experiment on NPs is the turbulence in applied liquid at the side of NP opposite to the solution application side that could have a variable effect on the kinetics of the recorded responses (refer to Supplementary Section 2 for numerical data). These factors introduce a large variability to experimental readouts obtained in different recordings and may make the data hardly interpretable. To cope with that, we applied control and experimental sets of chemicals on the same patch and then used the ratios of fitting coefficients for components with fast and slow decay time constants (τ) rather than absolute values of amplitudes and/or τ.

Acquisition and analysis

Recordings were obtained using a Multi-Clamp 700B amplifier (Molecular Devices), filtered at 4–8 kHz, digitized at 10 kHz and stored on a PC. pClamp/Clampfit 10 × software (Molecular Devices) was used for data storage and off-line analysis. For nonlinear fitting of single- and double-Gaussian and double-exponential functions, we used Wolfram Mathematica 10 software package.

Analysis of tonic currents

For analysis of tonic whole-cell currents, mean values of holding current were averaged at 30 s intervals. The shift of the tonic current was calculated as the difference between the holding current values (ΔI_{hold}) measured at stable baseline intervals before and after the application of an antagonist/channel blocker. The tonic s-GABAAR-mediated current was measured as the outward shift in

holding current following application of PTX (50 μM) in the continued presence of SR (25 μM).

Changes in root mean square (RMS) noise have also been used to reflect changes in tonic GABA$_A$R-mediated conductance and have been used because they are unaffected by current drift. Although RMS noise decreased in experiments in which tonic currents were blocked, this measurement is confounded by the presence of synaptic currents. Moreover, RMS noise is nonlinearly related to current and can paradoxically decrease when tonic currents increase[48]. We, therefore, only used RMS noise as a measure in experiment in which we were trying to block the tonic current. The values of the RMS noise were calculated for 200 ms epochs free of synaptic events. The change of RMS noise (ΔRMS) was calculated as the difference between the values before and after the application of antagonist(s). We obtained RMS noise values with calculation algorithms built-in into Clampfit 10 software.

Inhibitory charge transfer with phasic events and through tonically open s-GABA$_A$Rs was obtained as $Q_{ph} = F \times Q_{AV-ph} \times \Delta t$ and $Q_t = \Delta I_{hold} \times \Delta t$, respectively. Here Q_{ph}—overall phasic charge transfer, F—frequency of phasic events; Q_{AV-ph}—average charge transferred with individual phasic event (area under event's curve); Q_t—overall tonic charge transfer, ΔI_{hold}—difference between holding current under SR and SR + PTX; Δt—time interval over which charge transfer was calculated; see Fig. 1a for graphical representation.

Synaptic events were automatically detected and stored with Clampfit 10 detection algorithm. For spontaneous IPSCs area under curve was calculated for the space between the event peak and baseline obtained as average current for 3 ms before the IPSC occurrence. For tonic current, the area under the curve was calculated by the ΔI_{hold} multiplied by the time (60 s).

Analysis of the single-channel recordings

Application of GABA at outside-out patches (OOPs) and nucleated patches (NPs) evoked single-channel openings to two conductance levels: 37.2 ± 6.4 pS and 17 ± 9.3 pS (see Figs. 2a and 3a). The larger conductance level contributed 92.8% of the single-channel current, whereas subconductance level contributed 7.2% of the current; thus, the larger main conductance level was used when (possible) changes of single-channel conductance were compared under different experimental conditions.

The opening frequency of GABA$_A$R channels was calculated as $N/\Delta t$, where N is the number of openings and Δt is the time of recording. N was counted using a detection threshold of 1.6 pA more negative than the mean baseline and a minimum opening time of 0.4 ms.

It was virtually impossible to determine accurately the number of channels in a membrane patch; however, in our preparation, the vast majority of channel openings

were single-level events. In a case where there were multiple levels of channel openings, only the level with the highest conductance was analysed. This prevented us from overestimating opening-frequency increase, since in multi-channel patch, increased opening frequency would be accompanied by increase of proportion of multi-level events. Values for the average open-time of single channel were obtained with threshold-detection algorithm of Clampfit 10 × software.

To calculate and visualize the average open-time characteristic for different receptor subtypes, we constructed all-points histograms and fitted them with a double-Gaussian function:

$$F = \frac{p_1 e^{-\frac{(n-m_1)^2}{2\sigma_1^2}}}{\sigma_1 \sqrt{2\pi}} + \frac{p_2 e^{-\frac{(n-m_2)^2}{2\sigma_2^2}}}{\sigma_2 \sqrt{2\pi}}$$

where m_1 and m_2 are the mode values of Gaussians, σ_1 and σ_2 are the standard deviations of corresponding modes, n is the value of electrical current and p_1 and p_2 are the fitting constants. The general algorithm of multi-Gaussian histogram construction, fitting and interpretation were adapted from the works of Bennett and Kearns[49], and Traynelis and Jaramillo[48].

Analysis of phasic responses

Decay profiles of phasic responses recorded from NPs and whole-cell were fitted with double-exponential function

$$\Delta I = -a_1 e^{-\frac{t}{\tau_1}} - a_2 e^{-\frac{t}{\tau_2}}$$

where ΔI is a difference between the current recorded at baseline and at time t, e—the Euler's constant, a_1 and a_2—fitting constants and τ_1 and τ_2—decay time constants.

Data analysis in step current injection experiments

DGC input resistance was calculated as the gradient of the straight line best fitting the VI plot of the anti-peak voltage amplitude against the corresponding hyperpolarising current of 500 ms duration from −50 to −450 pA.

The value of DGC rheobase was measured in the experiment, where 1 s current injections with +5 pA incrementing steps were delivered until propagation of the first action potential.

Frequency of action potential generation (Hz) was measured at 0.5 s time intervals, where depolarizing current of 25–250 pA was injected in 25 pA steps.

Data analysis in coincidence detection experiment

Here, two stimulation electrodes were placed in the perforant path area, and the stimulation intensity was set so that when the two pathways were stimulated simultaneously, the patched DGC generated AP in ~50% of the

trials (threshold stimulation). After application of SR and SR + PTX, stimulation intensity at both electrodes was re-adjusted to match the spiking probability observed under the control. We then applied a single-Gaussian nonlinear fitting (similar approach as to open-time data from single-channel recordings) and used the changes of the standard deviation value (σ) for quantification of SR and SR + PTX effect on coincidence detection window.

GABA receptor antagonists, MCPG, CPPG, NPS, NBQX, CGP55845 and MDL-72222, were purchased from Tocris Bioscience. All other chemicals were purchased form Sigma-Aldrich. All data are given as mean ± standard error of mean. For statistical calculations, Student's paired t test, Student's unpaired t test, one-way and two-way analysis of variance (ANOVA) with Student–Newman–Keuls post hoc test were applied as indicated.

References
1. Ge, S. et al. GABA regulates synaptic integration of newly generated neurons in the adult brain. *Nature* **439**, 589–593 (2006).
2. Pavlov, I., Savtchenko, L. P., Kullmann, D. M., Semyanov, A. & Walker, M. C. Outwardly rectifying tonically active GABAA receptors in pyramidal cells modulate neuronal offset, not gain. *J. Neurosci.* **29**, 15341–15350 (2009).
3. Martin, L. J. et al. Alpha5GABAA receptor activity sets the threshold for long-term potentiation and constrains hippocampus-dependent memory. *J. Neurosci.* **30**, 5269–5282 (2010).
4. Duveau, V. et al. Spatiotemporal specificity of GABAA receptor-mediated regulation of adult hippocampal neurogenesis. *Eur. J. Neurosci.* **34**, 362–373 (2011).
5. Wlodarczyk, A. I. et al. GABA-independent GABAA receptor openings maintain tonic currents. *J. Neurosci.* **33**, 3905–3914 (2013).
6. McCartney, M. R., Deeb, T. Z., Henderson, T. N. & Hales, T. G. Tonically active GABAA receptors in hippocampal pyramidal neurons exhibit constitutive GABA-independent gating. *Mol. Pharmacol.* **71**, 539–548 (2007).
7. Wuarin, J. P. & Dudek, F. E. Electrographic seizures and new recurrent excitatory circuits in the dentate gyrus of hippocampal slices from kainate-treated epileptic rats. *J. Neurosci.* **16**, 4438–4448 (1996).
8. Raol, Y. H. et al. Enhancing GABA(A) receptor alpha 1 subunit levels in hippocampal dentate gyrus inhibits epilepsy development in an animal model of temporal lobe epilepsy. *J. Neurosci.* **26**, 11342–11346 (2006).
9. Palma, E. et al. Anomalous levels of Cl- transporters in the hippocampal subiculum from temporal lobe epilepsy patients make GABA excitatory. *Proc. Natl Acad. Sci. USA* **103**, 8465–8468 (2006).
10. Pavlov, I. et al. Progressive loss of phasic, but not tonic, GABAA receptor-mediated inhibition in dentate granule cells in a model of post-traumatic epilepsy in rats. *Neuroscience* **194**, 208–219 (2011).
11. Cohen, I., Navarro, V., Clemenceau, S., Baulac, M. & Miles, R. On the origin of interictal activity in human temporal lobe epilepsy in vitro. *Science* **298**, 1418–1421 (2002).
12. Glykys, J. et al. Differences in cortical versus subcortical GABAergic signaling: a candidate mechanism of electroclinical uncoupling of neonatal seizures. *Neuron* **63**, 657–672 (2009).
13. Cope, D. W. et al. Enhanced tonic GABAA inhibition in typical absence epilepsy. *Nat. Med.* **15**, 1392–1398 (2009).
14. Leutgeb, J. K., Leutgeb, S., Moser, M.-B. & Moser, E. I. Pattern separation in the dentate gyrus and CA3 of the hippocampus. *Science* **315**, 961–966 (2007).
15. Kemp, A. & Manahan-Vaughan, D. The hippocampal CA1 region and dentate gyrus differentiate between environmental and spatial feature encoding through long-term depression. *Cereb. Cortex* **18**, 968–977 (2008).
16. Bianchi, M. T. & Macdonald, R. L. Agonist trapping by GABAA receptor channels. *J. Neurosci.* **21**, 9083–9091 (2001).
17. Chang, Y. & Weiss, D. S. Allosteric activation mechanism of the alpha 1 beta 2 gamma 2 gamma-aminobutyric acid type A receptor revealed by mutation of the conserved M2 leucine. *Biophys. J.* **77**, 2542–2551 (1999).
18. Neelands, T. R., Fisher, J. L., Bianchi, M. & Macdonald, R. L. Spontaneous and gamma-aminobutyric acid (GABA)-activated GABA(A) receptor channels formed by epsilon subunit-containing isoforms. *Mol. Pharmacol.* **55**, 168–178 (1999).
19. Das, P., Bell-Horner, C. L., Machu, T. K. & Dillon, G. H. The GABA(A) receptor antagonist picrotoxin inhibits 5-hydroxytryptamine type 3A receptors. *Neuropharmacology* **44**, 431–438 (2003).
20. Das, P. & Dillon, G. H. Molecular determinants of picrotoxin inhibition of 5-hydroxytryptamine type 3 receptors. *J. Pharmacol. Exp. Ther.* **314**, 320–328 (2005).
21. Heaulme, M. et al. Biochemical characterization of the interaction of three pyridazinyl-GABA derivatives with the GABAA receptor site. *Brain Res.* **384**, 224–231 (1986).
22. Mortensen, M., Ebert, B., Wafford, K. & Smart, T. G. Distinct activities of GABA agonists at synaptic- and extrasynaptic-type GABAA receptors. *J. Physiol.* **588**, 1251–1268 (2010).
23. Christie, S. B., Miralles, C. P. & De Blas, A. L. GABAergic innervation organizes synaptic and extrasynaptic GABAA receptor clustering in cultured hippocampal neurons. *J. Neurosci.* **22**, 684–697 (2002).
24. Krueppel, R., Remy, S. & Beck, H. Dendritic integration in hippocampal dentate granule cells. *Neuron* **71**, 512–528 (2011).
25. Kress, G. J., Dowling, M. J., Meeks, J. P. & Mennerick, S. High threshold, proximal initiation, and slow conduction velocity of action potentials in dentate granule neuron mossy fibers. *J. Neurophysiol.* **100**, 281–291 (2008).
26. Loup, F., Wieser, H.-G., Yonekawa, Y., Aguzzi, A. & Fritschy, J.-M. Selective alterations in GABAAA receptor subtypes in human temporal lobe epilepsy. *J. Neurosci.* **20**, 5401–5419 (2000).
27. Whiting, P. J. GABA-A receptor subtypes in the brain: a paradigm for CNS drug discovery? *Drug Discov. Today* **8**, 445–450 (2003).
28. Bethmann, K., Fritschy, J.-M., Brandt, C. & Löscher, W. Antiepileptic drug resistant rats differ from drug responsive rats in GABAA receptor subunit expression in a model of temporal lobe epilepsy. *Neurobiol. Dis.* **31**, 169–187 (2008).
29. Baptista-Hon, D. T., Gulbinaite, S. & Hales, T. G. Loop G in the GABAA receptor alpha1 subunit influences gating efficacy. *J. Physiol.* https://doi.org/10.1113/jp273752 (2016).
30. Kralic, J. E. et al. GABAA receptor alpha-1 subunit deletion alters receptor subtype assembly, pharmacological and behavioral responses to benzodiazepines and zolpidem. *Neuropharmacology* **43**, 685–694 (2002).

31. Nusser, Z., Sieghart, W. & Somogyi, P. Segregation of different GABAA receptors to synaptic and extrasynaptic membranes of cerebellar granule cells. *J. Neurosci.* **18**, 1693–1703 (1998).

32. Nusser, Z. & Mody, I. Selective modulation of tonic and phasic inhibitions in dentate gyrus granule cells. *J. Neurophysiol.* **87**, 2624–2628 (2002).

33. Kettenmann, H., Backus, K. H. & Schachner, M. γ-Aminobutyric acid opens Cl-channels in cultured astrocytes. *Brain Res.* **404**, 1–9 (1987).

34. Ffrench-Mullen, J. M., Tokutomi, N. & Akaike, N. The effect of temperature on the GABA-induced chloride current in isolated sensory neurones of the frog. *Br. J. Pharmacol.* **95**, 753–762 (1988).

35. Bright, D. P. & Smart, T. G. Protein kinase C regulates tonic GABAA receptor-mediated inhibition in the hippocampus and thalamus. *Eur. J. Neurosci.* **38**, 3408–3423 (2013).

36. Munakata, M., Jin, Y. H., Akaike, N. & Nielsen, M. Temperature-dependent effect of zolpidem on the GABAA receptor-mediated response at recombinant human GABAA receptor subtypes. *Brain Res.* **807**, 199–202 (1998).

37. Houston, C. M., Bright, D. P., Sivilotti, L. G., Beato, M. & Smart, T. G. Intracellular chloride ions regulate the time course of GABA-mediated inhibitory synaptic transmission. *J. Neurosci.* **29**, 10416–10423 (2009).

38. Deidda, G., Bozarth, I. F. & Cancedda, L. Modulation of GABAergic transmission in development and neurodevelopmental disorders: investigating physiology and pathology to gain therapeutic perspectives. *Front. Cell. Neurosci.* **8**, https://doi.org/10.3389/fncel.2014.00119 (2014).

39. Chen, Z. W. & Olsen, R. W. GABAA receptor associated proteins: a key factor regulating GABAA receptor function. *J. Neurochem.* **100**, 279–294 (2007).

40. Carver, C. M. & Reddy, D. S. Neurosteroid interactions with synaptic and extrasynaptic GABAA receptors: regulation of subunit plasticity, phasic and tonic inhibition, and neuronal network excitability. *Psychopharmacology* **230**, 151–188 (2013).

41. Wettschureck, N. & Offermanns, S. Mammalian G proteins and their cell type specific functions. *Physiol. Rev.* **85**, 1159–1204 (2005).

42. Schoepp, D. D. & Conn, P. J. Metabotropic glutamate receptors in brain function and pathology. *Trends Pharmacol. Sci.* **14**, 13–20 (1993).

43. Nakanishi, S. et al. Glutamate receptors: brain function and signal transduction. *Brain Res. Rev.* **26**, 230–235 (1998).

44. Sylantyev, S. & Rusakov, D. A. Sub-millisecond ligand probing of cell receptors with multiple solution exchange. *Nat. Protoc.* **8**, 1299–1306 (2013).

45. Newland, C. F. & Cull-Candy, S. G. On the mechanism of action of picrotoxin on GABA receptor channels in dissociated sympathetic neurones of the rat. *J. Physiol.* **447**, 191–213 (1992).

46. Wachowiak, M. & Ache, B. W. Multiple inhibitory pathways shape odor-evoked responses in lobster olfactory projection neurons. *J. Comp. Physiol. A* **182**, 425–434 (1998).

47. Karnup, S. V. Background firing in cortical neurons with blockade of synaptic inhibition in guinea pig neocortical slices maintained in vitro. *Neurophysiology* **21**, 13–19 (1989).

48. Traynelis, S. F. & Jaramillo, F. Getting the most out of noise in the central nervous system. *Trends Neurosci.* **21**, 137–145 (1998).

49. Bennett, M. R. & Kearns, J. L. Statistics of transmitter release at nerve terminals. *Prog. Neurobiol.* **60**, 545–606 (2000).